ANL/NE-18/8

Preliminary SAM Assessment

Nuclear Engineering Division

About Argonne National Laboratory
Argonne is a U.S. Department of Energy laboratory managed by UChicago Argonne, LLC under contract DE-AC02-06CH11357. The Laboratory's main facility is outside Chicago, at 9700 South Cass Avenue, Argonne, Illinois 60439. For information about Argonne and its pioneering science and technology programs, see www.anl.gov.

ANL-NE-18/8

Preliminary SAM Assessment

prepared by
Rui Hu
Nuclear Engineering Division, Argonne National Laboratory

March 2018

ABSTRACT

The System Analysis Module (SAM) is a modern system analysis tool being developed at Argonne National Laboratory (Argonne) for advanced non-LWR safety analysis. To assist NRC to assess SAM capabilities for advanced reactor safety analysis and licensing at the NRC, a series of verification and other standard tests (OSTs) are modeled in SAM and code simulation results are compared with available analytical results. This report documents the preliminary SAM assessment using a matrix of six test problems. Each test problem is further examined with different boundary conditions, system configurations, or modeling options. Although relatively simple, these tests cover the basic equation models, basic component models, and basic system level processes and phenomena that must be modeled for advanced reactor safety analyses.

Table of Contents

LIST OF FIGURES

LIST OF TABLES

1 Introduction

The System Analysis Module (SAM) [1] is an advanced system analysis tool being developed at Argonne National Laboratory for advanced non-LWR safety analysis. It aims to be a modern system analysis code that takes advantage of the advancements in computing power, software design, numerical methods, and physical models over the past two decades. SAM focuses on modeling advanced reactor concepts such as SFRs (sodium fast reactors), LFRs (lead-cooled fast reactors), FHRs (fluoride-salt-cooled high temperature reactors) or MSRs (molten salt reactors), and HTGRs (high temperature gas-cooled reactors). These advanced concepts are distinguished from light-water reactors in their use of single-phase, low-pressure (liquid-metal and salt cooled), high-temperature, and non-unit Prandtl number coolants. These simple yet fundamental changes have significant impacts on core and plant design, the types of materials used, component design and operation, fuel behavior, and the significance of the fundamental physics in play during transient plant simulations.

This work supports the evaluation of the SAM code for advanced reactor safety analysis and licensing at the NRC. Although the transient simulation capabilities of typical reactor accidents have been demonstrated, continued verification and validation efforts are required to enhance code capabilities and maturation as a modern system code for advanced reactor safety analysis. The outcome of this assessment is expected to set the foundation for future collaboration in safety code and analysis method developments under the joint support of DOE and NRC.

2 Proposed Test Matrix

A hierarchy of tests, known as basic tests, separate effects tests, and integral effects tests (including operating nuclear reactor data), will be performed to comprehensively validate the SAM code. However, the objective of this work is not to perform an extensive validation of SAM, but to provide an initial assessment of SAM for system-level thermal fluid modeling capabilities and to facilitate the independent assessment of the code by NRC staff. These simple test problems will also help NRC staff become more familiar with the SAM code and gain experience with modeling using SAM.

Due to the limited scope, this work focuses primarily on the so-called other standard tests (OSTs) [2]. This element of validation compares code-calculated results with standards that do not employ experimental data. It encompasses tests of specific code features or functions; comparisons to equilibrium, concept problems with known outcomes, or analytical problems with known solutions; and problems to test the properties of the numerical solution methods. A total of six test problems have been identified, including:

1) Heat conduction in heat structures
2) Channel flow with direct coolant heating
3) Core channel flow and heat transfer
4) Heat exchanger modeling
5) Oscillating manometer
6) Natural circulation in a flow loop.

Each test is simulated with different boundary conditions, system configurations, or modeling options. Although relatively simple, these tests examine the basic equation models, basic component models, and basic system level processes and phenomena that must be modeled for advanced reactor safety analyses. The relevant thermal-fluid phenomena included in the test matrix are summarized in Table 2-1. All are of high importance to model reactor transients including Anticipated Operational Occurrence (AOO), Design Basis Accident (DBA) and Beyond Design Basis Accidents (BDBA).

Table 2-1.List of Phenomena for Computational Model of Interest

Phenomena	**Description**	**Test No.**
Heat transfer	Heat conduction in solid structures and convective heat transfer between structures and fluid flow	1, 3, 4
Single phase transient flow	Single-phase fluid dynamics corresponding the changes of system operation and boundary conditions.	2, 3, 5
Thermal inertia	The slower thermal response in solid heat structures due to heat capacities.	3, 6
Pump coast-down	Pump characteristics after a loss of power.	6
Transition to natural circulation	The fluid system loses the pumping power, and re-establishes the circulation relying on the gravity driving head from the density difference between the hot and cold fluid.	6

3 Heat conduction in Heat Structures

3.1 Introduction

The purpose of this assessment is to examine the modeling of the basic heat conduction equation. SAM simulation results are compared with the available analytical solutions. A large number of simulations are performed. The 1-D radial heat conduction equations and the 2-D axial-radial heat conduction equations in both Cartesian and Cylindrical coordinates are evaluated. Mesh convergence studies are also performed to demonstrate the high-order numerical discretization schemes used in SAM.

3.2 Model Descriptions and Analytical Solutions

3.2.1 1-D Radial Conduction

The 1-D radial steady-state conduction equation was solved for a generic long fuel plate or fuel pin, as illustrated in Figure 3-1, in both Cartesian and Cylindrical coordinates. The heat structure has a length of 10 cm and width (or radius) of 1 cm. It has a uniform volumetric heat source of 50 MW/m^3, and constant thermal conductivity of 16 W/mK. The adiabatic boundary condition was assumed at the left boundary, and fixed temperature boundary condition ($T_{bc} = 628.15\ K$) was assumed at the right boundary.

For plate fuel, the centerline (adiabatic boundary at the left surface) temperature can be calculated as:

$$T_{cl} = T_{bc} + \frac{q'''t^2}{2k} = 784.400\ K \tag{3-1}$$

For cylindrical fuel, the centerline (adiabatic boundary at the left surface) temperature can be calculated as:

$$T_{cl} = T_{bc} + \frac{q'''r^2}{4k} = 706.275\ K \tag{3-2}$$

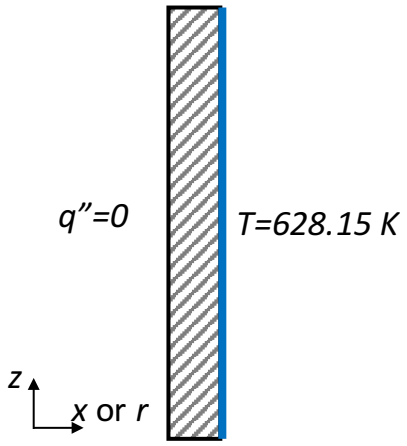

Figure 3-1. SAM model of the 1-D heat conduction problem

3.2.2 2-D Radial and Axial Conduction in a Cylinder

The 2-D radial and axial steady-state conduction equation was solved for a generic long solid rod, as illustrated in Figure 3-2. The same case is also included in the TRACE fundamental validation cases [5]. The heat structure has a length of 20 cm and radius of 5 mm. It has a uniform heat source of 1000 W distributed within the rod, and constant thermal conductivity of 2 W/mK. The solid rod is immersed in a pool of water having a constant temperature of 300 K in the bottom 10 cm and 500 K in the top 10 cm. A constant heat transfer coefficient of 1000 W/m^2K is applied to the outer surface of the rod. The tabulated analytical solution values from Table A.1.2 of Reference [5] are used here in Table 3-2 for comparison to the temperatures calculated by SAM.

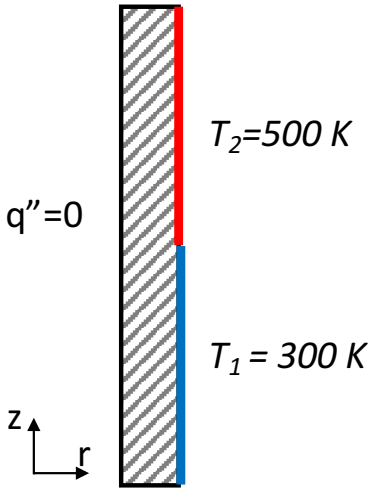

Figure 3-2. SAM model of the 2-D heat conduction problem

3.3 SAM Simulation Results

The SAM heat structure component (*PBCoupledHeatStructure*, see Table A-1) is used to model the above heat conduction problems. The test cases listed in Table 3-1 were evaluated with different geometries, boundary conditions, and modeling options. Steady state solutions were obtained in SAM for all test cases, and compared with the analytical solutions.

Table 3-1. SAM Test Cases of the Heat Conduction Modeling

Test Cases	Geometry	Boundary Conditions	Finite element type	Note
Case 1.1	plate	Left: adiabatic Right: constant temperature	first-order	Mesh sensitivity study performed
Case 1.2.1	cylinder	Left: adiabatic Right: constant temperature	first-order	Mesh sensitivity study performed
Case 1.2.2	cylinder	Left: adiabatic Right: constant temperature	second-order	Mesh sensitivity study performed
Case 1.3	cylinder	Left: adiabatic Right: convection with axially variable ambient temperature	second-order	

3.3.1 1-D Radial Conduction in a plate

For Test Case 1.1, the radial temperature distributions from various spatial discretizations are shown in Figure 3-3. With the increase of the node numbers, the distributions of SAM simulation results became closer to the analytical solutions. This is expected as at the steady-state, the temperature distribution in the heated plate is a perfect parabolic and need a large number of linear elements to fully resolve the parabolic distribution. It is also found that SAM simulation results are exactly the same as the analytical solution at all nodes, and not sensitive to the nodalization scheme used in the simulation.

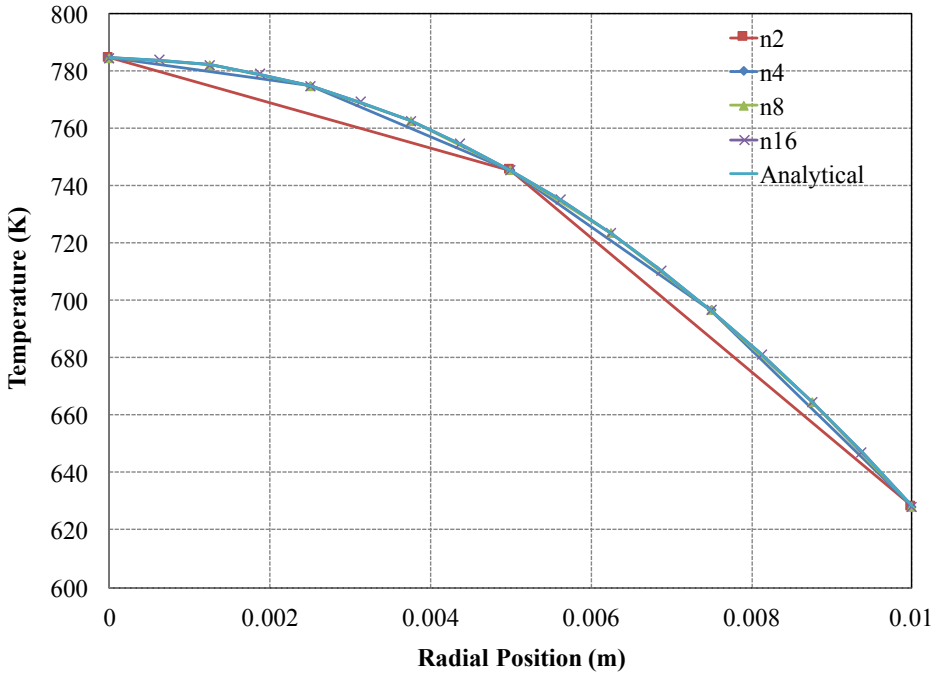

Figure 3-3. Comparisons of radial temperature distributions of the heated plate

3.3.2 1-D Radial Conduction in a cylinder

For Test Case 1.2, both first-order elements (Case 1.2.1) and second-order elements (Case 1.2.2) were applied for this test problem. The radial temperature distributions from various spatial discretizations are shown in Figure 3-4. It is seen that errors still exists with 40 radial elements if using first-order shape function, while no errors were observed even with a single radial element if using second-order shape function.

When comparing the centerline temperature predictions with the analytical results for the cases using first-order elements, the errors from various spatial discretizations are shown in Figure 3-5. The error drops with the increase number of radial elements. The second-order accuracy in spatial discretization is demonstrated from the error trend line for the cases using first-order elements.

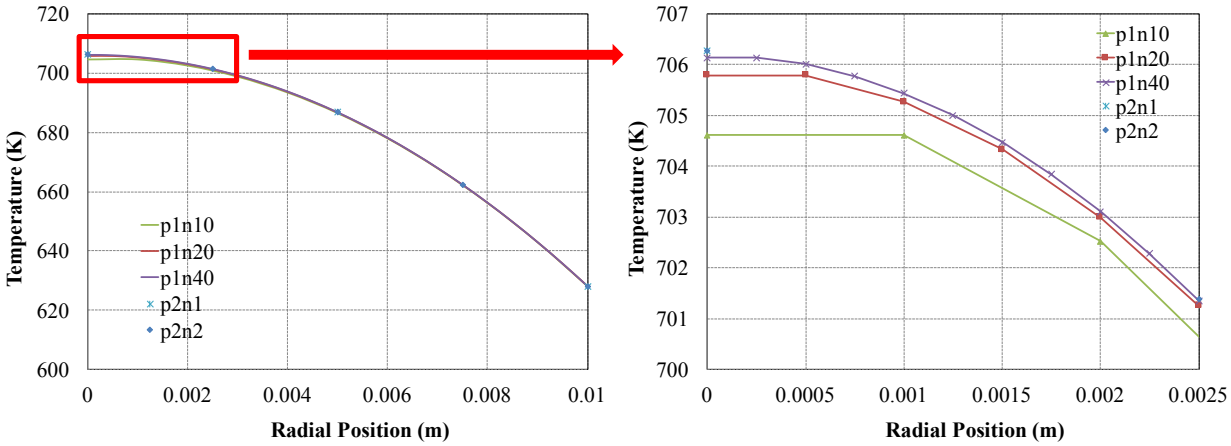

Figure 3-4. Comparisons of radial temperature distributions of the heated rod

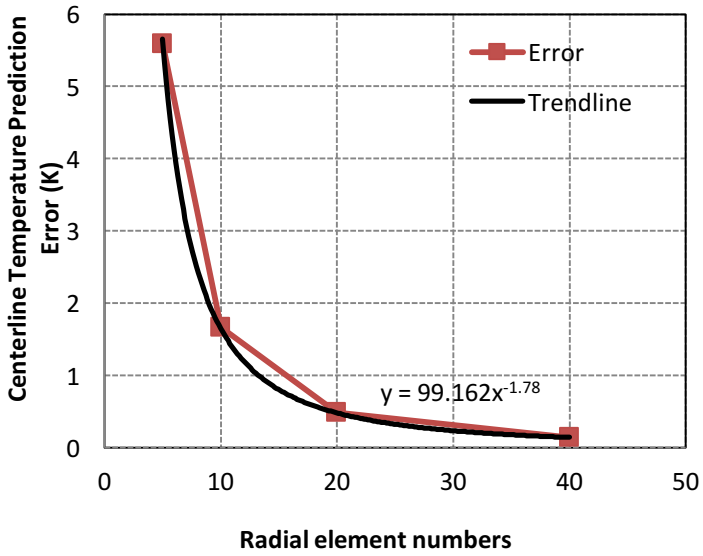

Figure 3-5. Spatial convergence for fuel centerline temperature, first-order finite elements

3.3.3 2-D Radial and Axial Conduction in a cylinder

The SAM simulation was run with Steady solver for this test case. The calculated steady-state conditions and analytical solution of centerline temperature distributions are compared in Table 3-2 and shown in Figure 3-6. The results given in Table 3-2 demonstrate that the SAM solutions of the 2-D heat-conduction equation are accurate. The largest errors are where temperature profile is steepening. Note that a relative coarse mesh, 40 (20-axial and 2-radial) elements total, was used in SAM simulations. The errors can be reduced if a finer mesh is used.

Table 3-2. Comparison of SAM and Analytical Solutions for the Steady State Axial-Radial Heat Conduction Problem

Location (m)	Analytical (K)	SAM (K)	Error (K)
0	658.1	658.1	0.0
0.01	658.1	658.1	0.0
0.02	658.1	658.1	0.0
0.03	658.1	658.1	0.0
0.04	658.1	658.1	0.0
0.05	658.1	658.1	0.0
0.06	658.1	658.1	0.0
0.07	658.1	658.1	0.0
0.08	658.2	658.2	0.0
0.09	662.7	662.3	-0.4
0.1	758.1	758.1	0.0
0.11	853.9	853.9	0.0
0.12	857.9	858.0	0.1
0.13	858.1	858.1	0.0
0.14	858.1	858.1	0.0
0.15	858.1	858.1	0.0
0.16	858.1	858.1	0.0
0.17	858.1	858.1	0.0
0.18	858.1	858.1	0.0
0.19	858.1	858.1	0.0

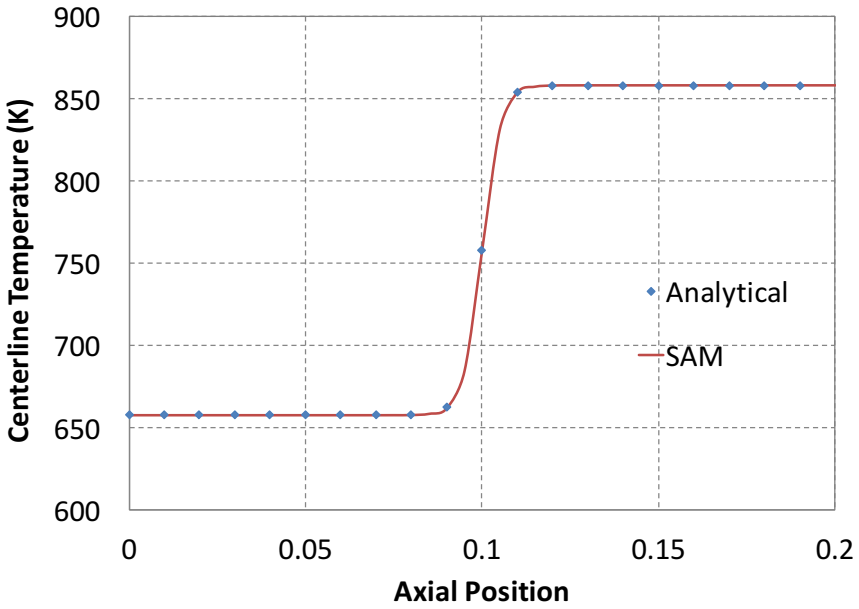

Figure 3-6. Comparisons of centerline temperature distributions of the heated rod, 2D conduction

3.4 Assessment Results Summary

Radial and Radial-Axial heat conduction problems were simulated with SAM, and found to be in excellent agreement with the analytical solutions for the problems, demonstrating that the heat conduction modeling in SAM is accurate. The effects of different spatial and element-order schemes are investigated. It is found that the use of second-order finite elements would significantly increase the efficiency and accuracy of the simulations for cylindrical heat structures.

4 Fluid Flow in a Channel

4.1 Introduction

The purpose of this assessment is to examine the modeling of the basic single-phase flow in a flow channel. Direct coolant heating is assumed. SAM simulation results are compared with analytical solutions. A number of simulations have been performed with variable boundary conditions, including both steady state and transient simulations. Temporal and spatial convergence studies are also performed to demonstrate the high-order numerical discretization schemes used in SAM.

4.2 Model Descriptions and Analytical Solutions

4.2.1 1-D Steady Flow

The 1-D fluid flow model was tested for a generic 1-D channel flow, with geometry and boundary conditions specified in Table 4-1.

Table 4-1. Geometry and Boundary Conditions of a Single-phase Flow Test

Parameters	**Values**
Hydraulic Diameter (m)	0.02
Length (m)	1
Flow Area (m^2)	0.000314
Heat Source (W^3)	User-defined function
Inlet velocity (m/s)	0.005, 0.5, 50
Inlet temperature (K)	628 or user-defined function

Equation 4-1 presents a reduced form of the energy equation at steady-state in a flow channel with constant flow area. The terms for axial conduction, pressure gradient, and friction dissipation are neglected.

$$\dot{m}\frac{d}{dz}\,h_m = q'(z) \tag{4-1}$$

In this equation $\dot{m}$ is mass flow rate, h_m is specific enthalpy of the fluid, and $q'(z)$ is the linear heat generation rate. Assuming constant fluid specific heat, integrating this equation over the axial length gives the following fluid temperature solution:

$$T(z) = T_{in} + \frac{\int_0^z q'(z)\,dz}{\dot{m}\,c_p} = T_{in} + \frac{\int_0^z q'''(z)A\,dz}{\dot{m}\,c_p} \tag{4-2}$$

where c_p is the specific heat capacity of the fluid; T is the fluid temperature and T_{in} equals $T(0)$; and A is the cross-section flow area.

For the baseline case, a sine power shape is assumed: $q'''(z) = 10^8 \sin(\pi z)$. The resulting axial temperature distribution of the fluid flow is then given by:

$$T(z) = T_{in} + \frac{10^8 A}{\pi \dot{m}\,c_p}(1 - cos(\pi z)) \tag{4-3}$$

4.2.2 1-D Transient Flow

One challenging problem for traditional system codes, such as TRACE and RELAP-5, is to accurately model the wave oscillation or the sudden disturbance of the system. It was challenging to achieve robust numerical stabilities while minimizing numerical diffusions due to their first-order approximations of the differential equations in both time and space. An example of wave propagation problem is thus tested in SAM for a pipe flow problem. The flow channel geometry is the same as the one shown in Table 4-1, however, the inlet temperature oscillates following a sinusoidal distribution, $T_{in}(t) = 628 + 100sin\,(\pi t)$; the inlet velocity is fixed, $u_{in}(t) = 0.5\ m/s$; and the initial pipe temperate is at 628 K.

If the flow channel is unheated, the fluid temperature at any location z at ti*me* t can be linked with the inlet temperature:

$$T(z,t) = T(0, t - \frac{z}{u}), \tag{4-4}$$

in which u is the flow velocity. If the flow channel is heated, the fluid temperature at any location z at ti*me* t can be given as:

$$T(z,t) = T\left(0, t - \frac{z}{u}\right) + \frac{\int_0^z q'(z)\,dz}{\dot{m}\,c_p} \tag{4-5}$$

4.3 SAM Simulation Results

The SAM unit flow component (*PBOneDFluidComponent*) is used to model the above flow problem. The test cases listed in Table 4-2 were evaluated with different boundary conditions and heating conditions. Steady state solutions were obtained in SAM for Cases 2.1.1, 2.1.2 and 2.1.3; and transient solutions were obtained for Cases 2.1 and 2.2. The SAM simulation results were also compared with the available analytical solutions.

Table 4-2. SAM Test Cases of Single-phase Flow Modeling

Test Cases	Boundary Conditions	Heating	Note
Case 2.1.1 - Base case	Inlet: constant flow and temperature Outlet: constant pressure	Sine shape	Mesh sensitivity study performed
Case 2.1.2 - Low flow	Inlet: constant flow and temperature Outlet: constant pressure	Sine shape	
Case 2.1.3 - High flow	Inlet: constant flow and temperature Outlet: constant pressure	Sine shape	
Case 2.2.1 - Inlet temperature wave	Inlet: constant flow and variable temperature Outlet: constant pressure	None	Time integration scheme effects studied
Case 2.2.2 - Inlet temperature wave	Inlet: constant flow and variable temperature Outlet: constant pressure	Uniform	

4.3.1 1-D Steady Flow

For Test Case 2.1.1, the temperature distributions from SAM simulations with various spatial discretizations are shown in Figure 4-1. With the increase of the element numbers, the distributions of SAM simulation results became closer to the analytical solutions. The maximum temperature differences between SAM simulation and the analytical solutions are listed in Table 4-3. It is seen that the SAM simulation results are already very close to the analytical solution when using 20 elements for the 1-meter flow channel. The maximum errors from various spatial discretizations are also shown in Figure 4-2. The second order accuracy in spatial discretization is demonstrated from the error trend line. This is expected in SAM simulations when using first-order elements.

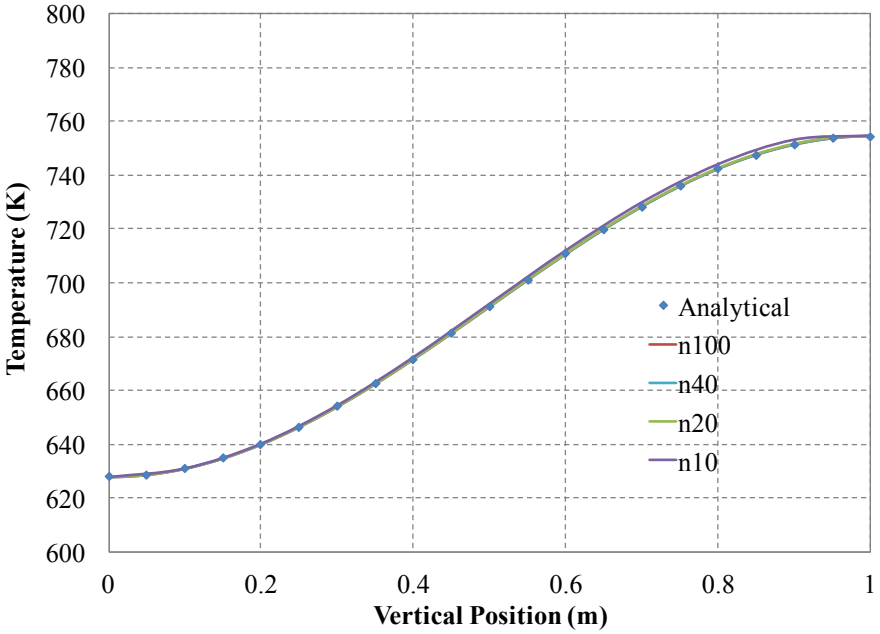

Figure 4-1. Comparisons of fluid temperature distributions, spatial discretization effects

Table 4-3. Maximum Differences between SAM and Analytical Results for Models with Various Element Numbers

Element numbers	Max. Temperature Errors (K)
100	0.02
40	0.13
20	0.52
10	2.05

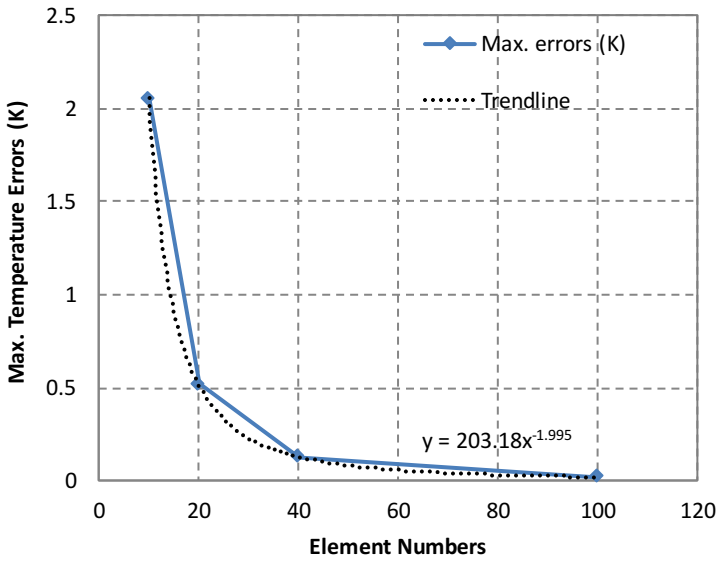

Figure 4-2. Spatial convergence for maximum temperature errors, Case 2.1.1 with first-order finite elements

Two similar cases were tests with different inlet velocity conditions, with one at 0.005 m/s and the other at 50 m/s. The volumetric heating power was also increased or decreased 100 times from the base case. The fluid temperature distribution in the channel will thus be unchanged. These two tests were designed to check the code performance under very high and very low flow conditions. The temperature distributions from SAM simulations with different inlet velocities are shown in Figure 4-3. All simulation results agree very well with the analytical solutions, indicating that the code performance is very good for a wide range of flow conditions.

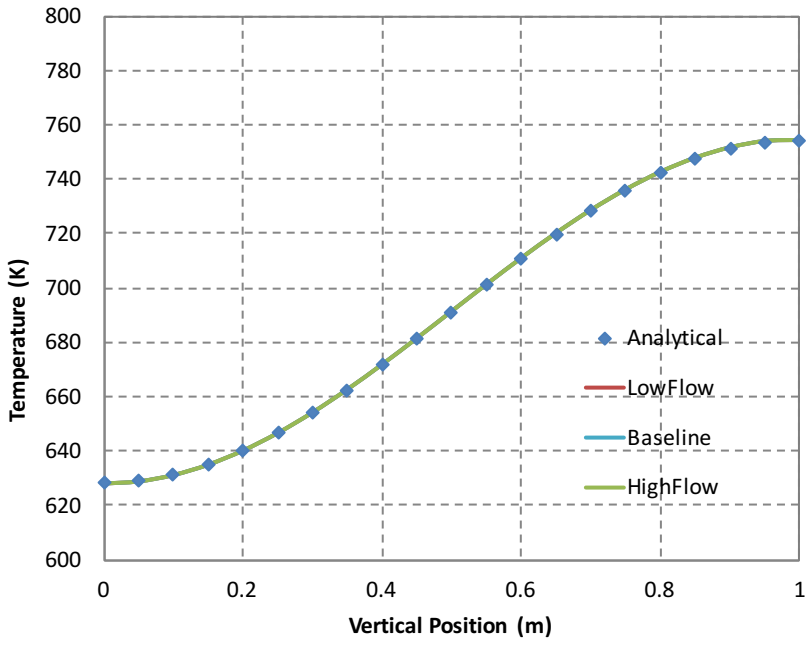

Figure 4-3. Comparisons of fluid temperature distributions, inlet velocity effects

4.3.2 1-D Transient Flow

The transient responses of the inlet temperature wave propagation are shown in Figure 4-4, where the SAM code predictions agreed very well with the analytical solutions. This is because of the high-order accuracy in both spatial and temporal discretization in SAM. The second-order backward differentiation formula (BDF2) is the default temporal discretization scheme in SAM. If the first-order time integration scheme (backward Euler) were used, numerical damping or diffusion would occur, as shown in Figure 4-5. Note that there is always some smoothing (numerical diffusion) at the wave propagation front because the temperature gradient of this test problem is not continuous (before $t = 2\ s$).

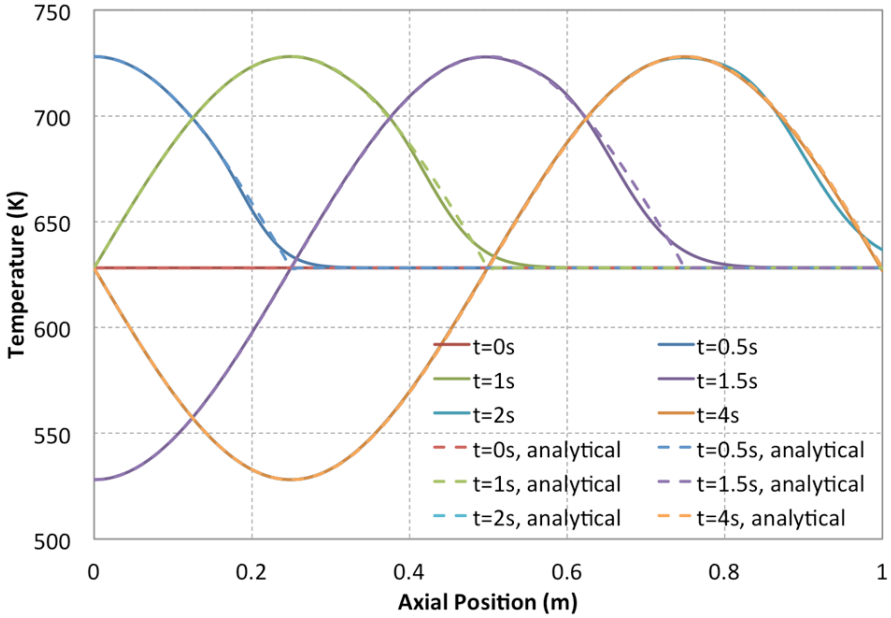

Figure 4-4. Transient responses of the pipe under inlet temperature oscillation, BDF2

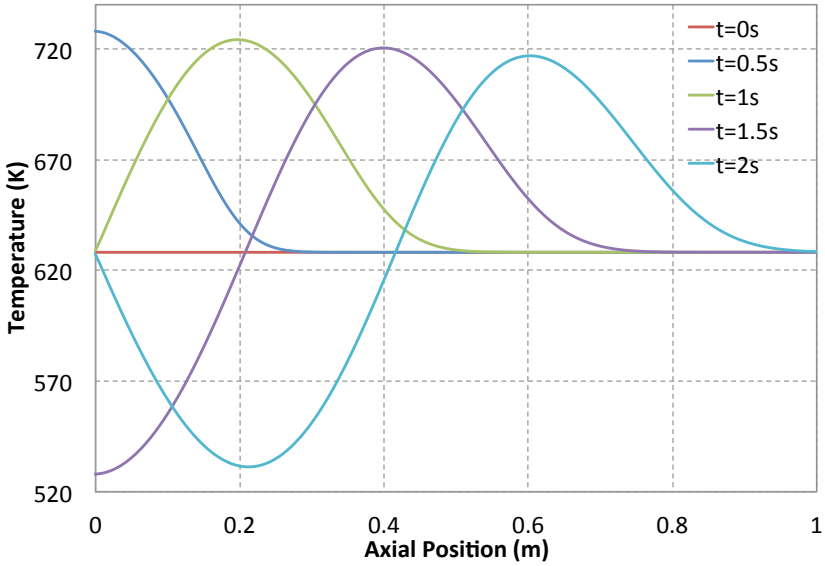

Figure 4-5. Damped temperature wave of the pipe under inlet temperature oscillation, backward Euler

Using different time step sizes, the outlet temperature responses from SAM simulations are shown in Figure 4-6. With the increase of the time step sizes, the SAM simulation results became more diffusive and further away from the analytical solutions. The differences of the channel outlet temperature between SAM simulation and the analytical solutions are also shown in Figure 4-7. It is shown that the order of temporal convergence rate is about 1.5 for this test problem, from the error trend line.

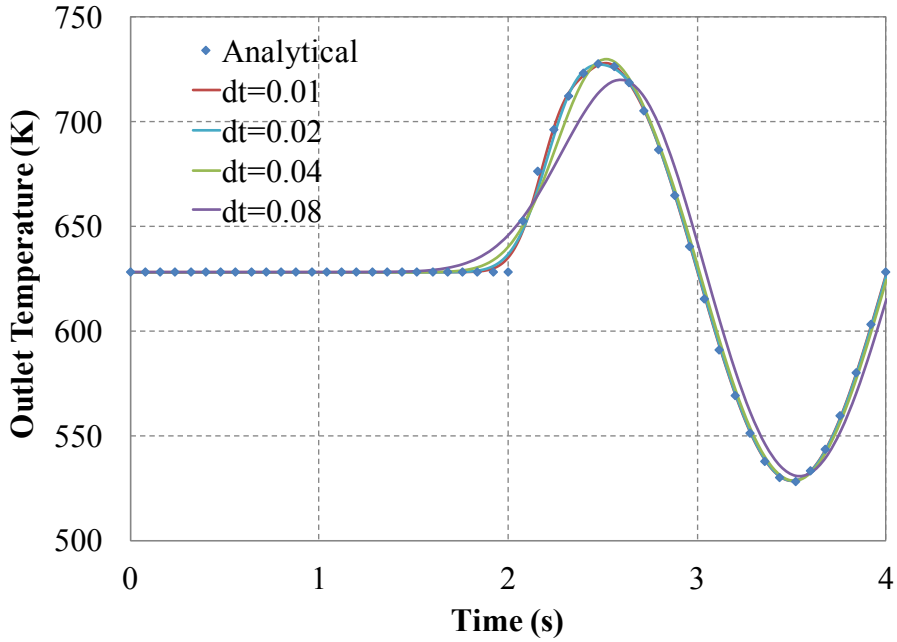

Figure 4-6. Comparisons of outlet temperature of Case 2.2.1, time step size effects

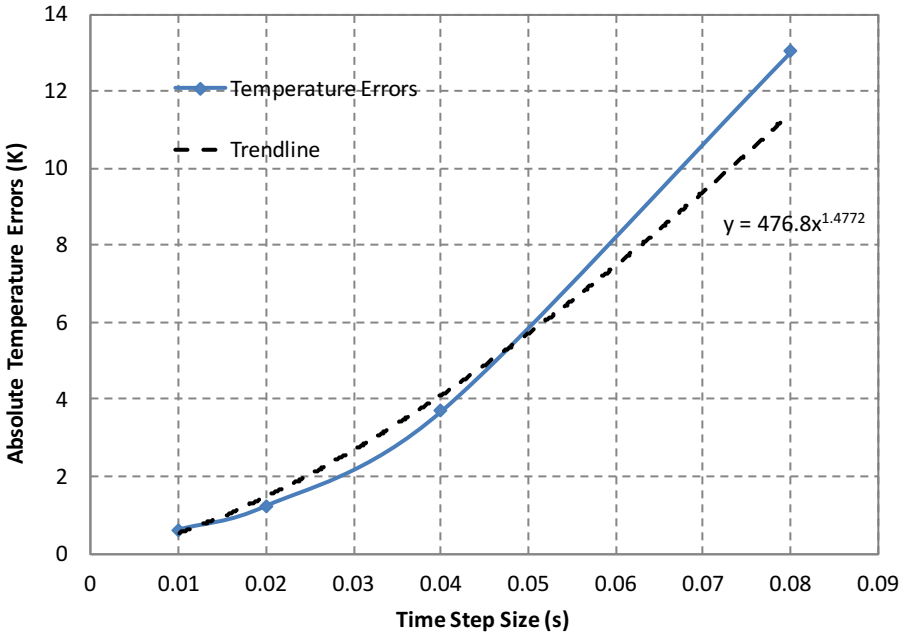

Figure 4-7. Temporal convergence for outlet temperature errors, Case 2.2.1 with BDF2 scheme

The inlet temperature wave propagation problem was also tested with the effects of direct fluid heating. The SAM transient responses are shown in Figure 4-8. The SAM code predictions of channel outlet temperature agreed very well with the analytical solutions, and the two plots cannot be distinguished from each other.

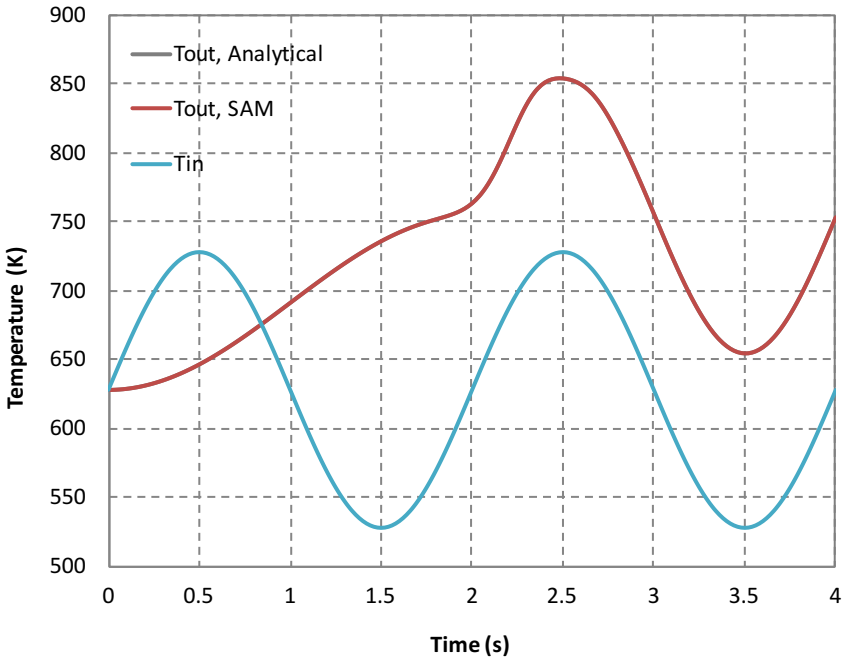

Figure 4-8. Transient responses of outlet temperature in Case 2.2.2

4.4 Assessment Results Summary

The basic single-phase flow modeling in a flow channel was tested with both steady and transient test problems. SAM simulation results were in excellent agreement with the analytical solutions for the problems, demonstrating that the basic fluid flow modeling in SAM is accurate. The effects of different nodalizations, time step sizes, and temporal schemes were investigated. The convergence rates of the high-order spatial and temporal discretization schemes in SAM have been confirmed by a series of verification tests. It was also found that the BDF2 time integration scheme can well resolve the temperature wave propagation problem because of its second-order accuracy and minimal numerical diffusion, while the first-order scheme (backward Euler) would cause significant numerical diffusion.

5 Core Channel Flow and Heat Transfer

5.1 Introduction

The purpose of this assessment is to examine the modeling of a core channel Component, which simulates the average coolant flow in rod bundles, heat conduction inside a fuel rod, and the convective heat transfer between the coolant and the fuel rod. SAM simulation results are also compared with the available analytical solutions. Both steady-state and transient simulation are performed. Transient simulation results are also compared with the results from test problem #2 (Case 2.2.2), channel flow with direct coolant heating.

5.2 Model Description and Analytical Solution

As discussed in Section 3, the second-order finite-element shape functions and mesh are suggested for high efficiency in SAM for modeling heat conduction in cylinders. Here, a core channel problem with uniform power distribution inside the fuel pin is presented to confirm its efficiency. The schematic of the spatial discretization of the core channel problem is shown in Figure 5-1. The different lines of colors on the left represent different heat structures in a fuel pin (i.e., fuel, gap, and clad). The fluid and solid domains exchange energy at the fluid-structure interface nodes. For the Steady test case, the inlet of the core channel flow is fixed at constant temperature and flow rate. Constant material thermophysical properties are assumed for this verification test. The geometry and boundary conditions of the fluid flow and the fuel pin are specified in Table 5-1. For the Transient test case, the inlet temperature oscillates following a sinusoidal distribution, $T_{in}(t) = 628.15 + 100sin\ (\pi t)$ and the inlet velocity is unchanged.

The analytical solutions of the Steady test problem can be easily derived, with coolant temperature:

$$T_{coolant}(z) = T_{in} + \frac{q'}{\dot{m}c_p} z \tag{5-1}$$

and the fuel centerline temperature:

$$T_{f\_cl}(z) = T_{in} + q' \left(\frac{z}{\dot{m}\, c_p} + \frac{1}{2\,\pi\,\mathrm{R_{co}}\, h_c} + \frac{1}{2\,\pi\, k_c} \ln\left(\frac{R_{co}}{R_{ci}}\right) + \frac{1}{2\,\pi\, k_c} \ln\left(\frac{R_{go}}{R_{gi}}\right) + \frac{1}{4\,\pi\, k_f} \right) \tag{5-2}$$

where h_c is the convective heat transfer coefficient of the flow, R_{co} and R_{ci} is the radii at the clad outer and inner surfaces, R_{go} and R_{gi} is the radii at the sodium gap outer and inner surfaces, and k_f is the thermal conductivity of the fuel pellet.

Table 5-1. Geometry and Boundary Conditions of the Core Channel Problem, Case 3.1

General		
Coolant Inlet Temp	K	628.15
Mass Flow Rate Per Pin	kg/s	0.15
Total Power	W	30000
Dimensions		
Fuel Height	m	0.8
Fuel Radius	m	3.02E-03
Cladding Inner Radius	m	3.48E-03
Cladding Outer Radius	m	4.00E-03
Hydraulic Diameter	m	3.18E-03
Coolant Flow Area	m^2	2.00E-05
Wetted Perimeter	m	2.51E-02
Thermo-Physical Properties		
Fuel Thermal Conductivity	W/m-K	16
Clad Thermal Conductivity	W/m-K	26
Gap Thermal Conductivity	W/m-K	64
Sodium Density	kg/m^3	865.51
Sodium Heat Capacity	J/kg-K	1272
Sodium Thermal Conductivity	W/m-K	72
Sodium Viscosity	Pa-s	2.62E-04
Other Values		
Heat Transfer Coefficient	W/m^2-K	1.60E+05
Friction Factor		0.017
Pressure at Core Outlet	Pa	2.00E+05

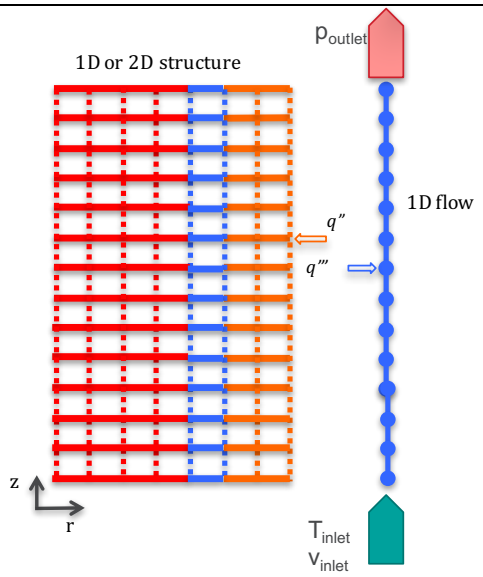

Figure 5-1. The schematic of the spatial discretization of the core channel problem

5.3 SAM Simulation Results

The SAM *PBCoreChannel* component is used to model the above core channel problem. The test cases listed in Table 5-2 were evaluated with different boundary conditions and spatial discretization schemes. Steady state solutions were obtained in SAM for Cases 3.1; and transient solutions were obtained for Cases 3.2. The SAM simulation results were also compared with the available analytical solutions.

Table 5-2. SAM Test Cases of Core Channel Flow

Test Cases	Boundary Conditions	Heating	Note
Case 3.1	inlet: constant flow and temperature outlet: constant pressure	Uniform	Base case; Spatial discretization schemes studied
Case 3.2	inlet: constant flow and variable temperature outlet: constant pressure	Uniform	Inlet temperature wave

5.3.1 Steady Simulations

Both first-order element and second-order element schemes were applied for Case 3.1. The errors between the code predictions and the analytical solutions are shown in Figure 5-2 and Figure 5-3 for fuel centerline temperatures and coolant temperatures, respectively. It is clearly seen that the errors from second-order elements simulation are essentially zero, even though only two radial elements were used for the fuel pellet region. However, the errors from the first-order element simulation remained notable when using 20 radial elements to model the fuel pellet.

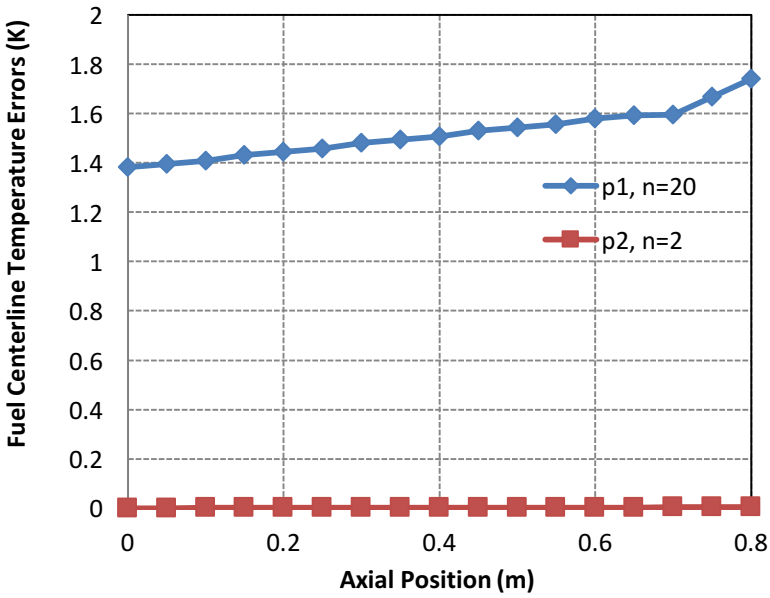

Figure 5-2. Errors of fuel centerline temperature predictions of a fuel assembly

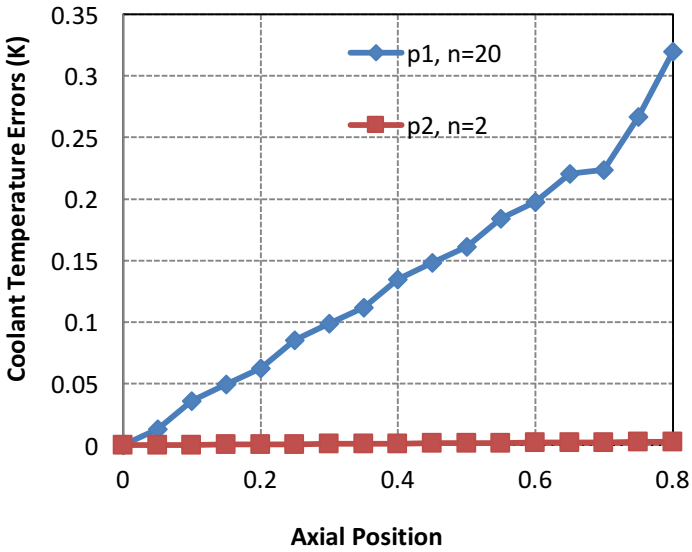

Figure 5-3. Errors of coolant temperature predictions of a fuel assembly

5.3.2 Transient Case with Inlet Temperature Wave

Similar to the test case discussed in Section 4.3.2, a transient case of PBCoreChannel flow with an inlet temperature wave was developed to examine the effects of solid thermal inertia during transients. Transient simulation results are compared with the results of the channel flow test problem with direct coolant heating. For consistency, the coolant channel geometry and flow conditions are exactly the same as the those of Case 2.2.2 in Table 4-2, and listed in Table 5-3.

The core inlet and outlet temperature responses during the transient are shown in Figure 5-4. For comparison, the channel outlet temperature of the direct coolant heating case is also included. It is seen that the core outlet temperature responded more slowly during the initial heating stage because of the time delay in heating up the solid structures. During the wave propagation stage, the oscillating magnitude of core outlet temperature is much smaller than that of the direct heating case. Again, this behavior is expected because of the thermal inertia of the solid fuel pin.

Table 5-3. Geometry and Boundary Conditions of the Core Channel Problem, Case 3.2

General		
Coolant Inlet Temperature	K	Sine function
Coolant Inlet Velocity	m/s	0.5
Total Power	W	9995
Dimensions		
Fuel Height	m	1
Fuel Radius	m	3.02E-03
Cladding Inner Radius	m	3.48E-03
Cladding Outer Radius	m	4.00E-03
Hydraulic Diameter	m	2.00E-02
Coolant Flow Area	m^2	3.14E-04
Thermo-Physical Properties		
Fuel Thermal Conductivity	W/m-K	16
Clad Thermal Conductivity	W/m-K	26
Gap Thermal Conductivity	W/m-K	64
Sodium Density	kg/m^3	800
Sodium Heat Capacity	J/kg-K	1260
Sodium Thermal Conductivity	W/m-K	60
Sodium Viscosity	Pa-s	2.0E-04
Other Values		
Heat Transfer Coefficient	W/m^2-K	1.60E+05
Friction Factor		0.017
Pressure at Core Outlet	Pa	2.00E+05

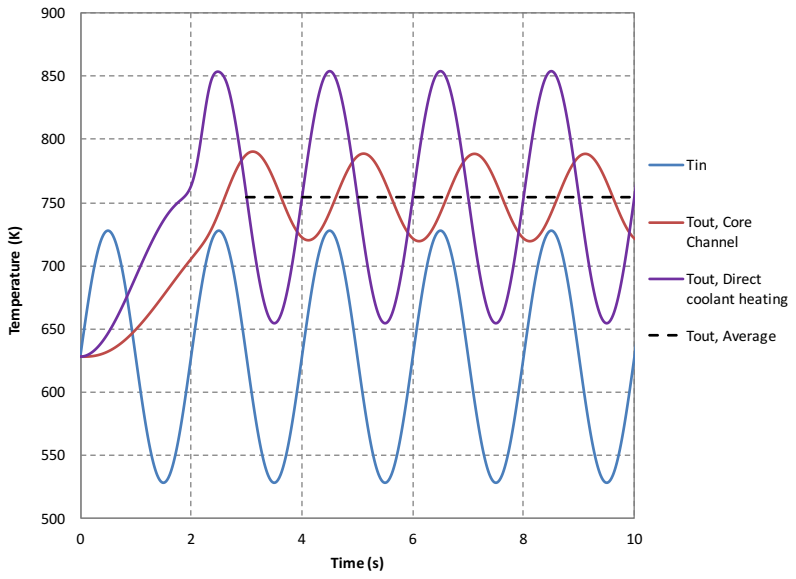

Figure 5-4. Transient responses of core outlet temperature, comparing with the case with direct coolant heating

5.4 Assessment Results Summary

The core channel Component, which simulates the average coolant flow in rod bundles, heat conduction inside a fuel rod, and the convective heat transfer between the coolant and the fuel rod, was tested with both steady and transient test problems. SAM simulation results were in excellent agreement with the analytical solutions for the Steady test problems, demonstrating that the basic convective heat transfer modeling between fluid flow and solid structures in SAM is accurate. The effects of different nodalization schemes were investigated. It is confirmed that the use of second-order finite elements would significantly increase the efficiency and accuracy of the simulations for cylindrical heat structures. Transient simulation results of the inlet temperature wave test case are compared with the results of the channel flow test problem with direct coolant heating. The expected smaller oscillating magnitude of core outlet temperature were observed because of the thermal inertia of the solid fuel pin.

6 Heat Exchanger Flow and Heat Transfer

6.1 Introduction

The purpose of this assessment is to examine the modeling of a heat exchanger Component, which simulates the fluid flow in the primary and secondary sides of a heat exchanger, convective heat transfer, and the heat conduction in the tube wall. SAM simulation results are compared with analytical solutions. A number of simulations were performed with variable configurations, including countercurrent and concurrent Heat Exchanger with plate or cylindrical tube walls.

6.2 Model Description

The design information of the intermediate heat exchanger (IHX) of the Advanced Burner Test Reactor [3] was used in this heat exchanger test problem. The inlet temperatures are 783 K and 606 K for the primary and secondary sides. The detailed geometry and boundary conditions of the heat exchanger are specified in Table 6-1.

Table 6-1. Geometry and Boundary Conditions of the Heat Exchanger Problem

General		
Primary Inlet Temperature	K	783.15
Secondary Inlet Temperature	K	606.15
Primary Mass Flow Rate	kg/s	632
Secondary Mass Flow Rate	kg/s	632
Dimensions		
Length	m	3.71
Primary Flow Area	m^2	0.766
Secondary Flow Area	m^2	0.517
Primary Hydraulic Diameter	m	0.0186
Secondary Hydraulic Diameter	m	0.014
Number of Heat Transfer Tubes	#	3300
Tube outer diameter	mm	15.9
Tube wall thickness	mm	0.889
Thermo-Physical Properties		
Tube Wall Thermal Conductivity	W/m-K	26.3
Tube Wall Density	kg/m^3	765
Tube Wall Heat Capacity	J/kg-K	638
Other Values		
Heat Transfer Coefficient – Primary Side	W/m^2-K	1.613E+05
Heat Transfer Coefficient – Secondary Side	W/m^2-K	1.613E+05

6.3 SAM Simulation Results

The SAM *PBHeatExchanger* component is used to model the above heat exchanger problem. The test cases listed in Table 6-2 were evaluated with different geometry conditions and heat exchanger types. Steady state solutions were obtained in SAM for all cases. The SAM simulation results were compared with the available analytical solutions.

Table 6-2. SAM Test Cases of Single-phase Flow Modeling

Test Cases	Structure geometry type	HX Type	Note
Case 4.1.1	Plate	countercurrent	Base case
Case 4.1.2	Plate	countercurrent	Half primary side flow; Spatial discretization sensitivity study performed
Case 4.2.1	Cylindrical	countercurrent	
Case 4.2.2	Cylindrical	concurrent	

In the base case simulation of the ABTR IHX, the heat exchanger tube wall is modeled as a plate because its thickness is very small comparing to the tube inner diameter. Because the flow rates are the same for the two sides, linear temperature distributions are expected for the two sides. The code predictions are shown in Figure 6-1. Assuming constant heat transfer coefficients for both sides of the heat exchanger, constant wall thermal conductivity, and constant specific heat capacity of the fluid, the analytical solution of the temperature difference between the primary and secondary sides of the heat exchanger can be obtained from Eq. 6-1.

$$ln\left(\frac{\Delta T(x)}{\Delta T(0)}\right) = -h_e P_h \left(\frac{1}{\dot{m}_p c_p} - \frac{1}{\dot{m}_s c_p}\right) x \qquad (6\text{-}1)$$

In which ΔT is the fluid temperature difference between the primary and secondary sides, P_h is the heated perimeter, $\dot{m}_p$ and $\dot{m}_s$ are the mass flow rates of both sides, c_p is the specific heat capacity, and h_e is the effective heat transfer coefficient between the primary and secondary side. If the tube wall is modeled as a plate, h_e can be defined as:

$$h_e = \frac{1}{\frac{1}{h_p} + \frac{t}{k} + \frac{1}{h_s}} \qquad (6\text{-}2)$$

In which, h_p and h_s are heat transfer coefficients in primary and secondary sides, respectively; and t and k are the thickness and thermal conductivity of the plate between primary and secondary sides, respectively.

To obtain a clear exponential distribution (as shown in Eq. 6-1) of the temperature difference, the mass flow rate of the primary side in the above heat exchanger problem is reduced to half for Case 4.1.2. The calculated and analytical fluid temperature differences between the primary and the secondary sides along the heat exchanger pipe are shown in Figure 6-2. A mesh convergence study has also been performed for this test problem. The number of axial pipe elements varies from 10, 20, to 40, while the radial element number of the wall remained unchanged at 4. The

comparison indicates that the simulation results agree well with the analytical solution, with a maximum error of temperature difference less than 1 °K for the case with the coarsest mesh (with 10 elements for the 3.7-meter-long heat exchanger).

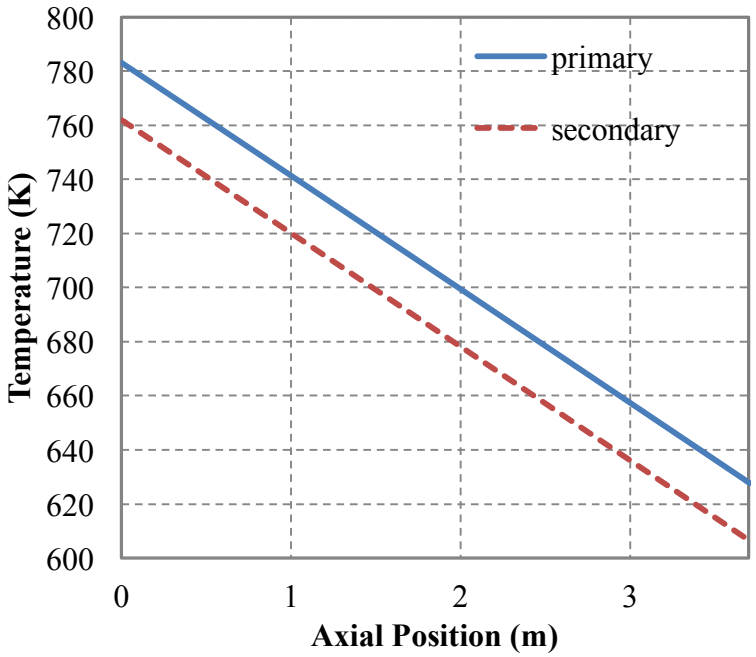

Figure 6-1. Temperature distribution of a counter-current heat exchanger, Case 4.1.1

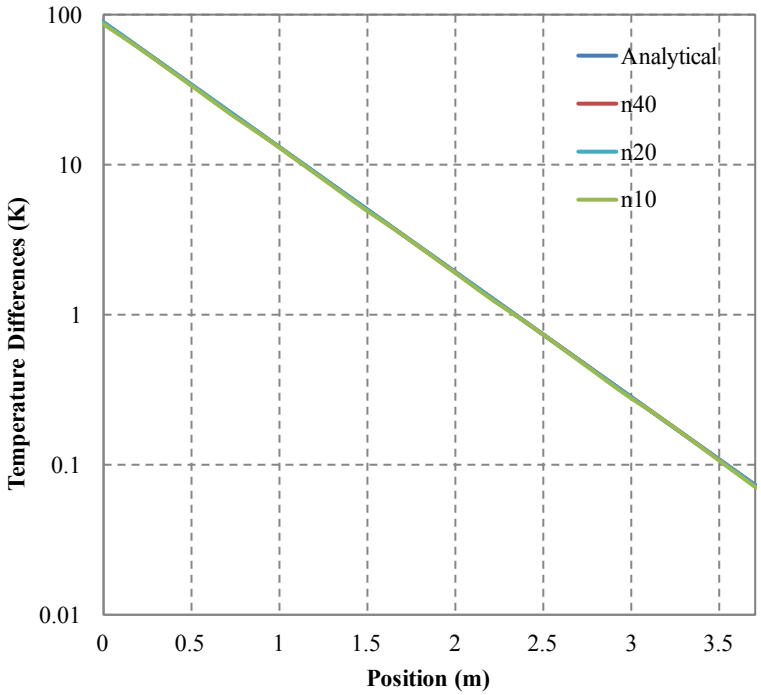

Figure 6-2. Temperature difference distribution of a counter-current heat exchanger, Case 4.1.2

To examine the effects of using a plate geometry to model the cylindrical tube wall, another case (Case 4.2.1) is developed to model the ABTR IHX tube wall with an annulus. All the other conditions remain the same. It was found that the SAM simulation results of the cylindrical tube are almost identical to those of the base case using a plate tube wall. The differences in fluid temperatures between the two simulations are shown in Figure 6-3, with the maximum temperature difference at about 0.15 K. It is thus confirmed that the assumption of using a plate to model the annulus tube wall of the IHX is valid.

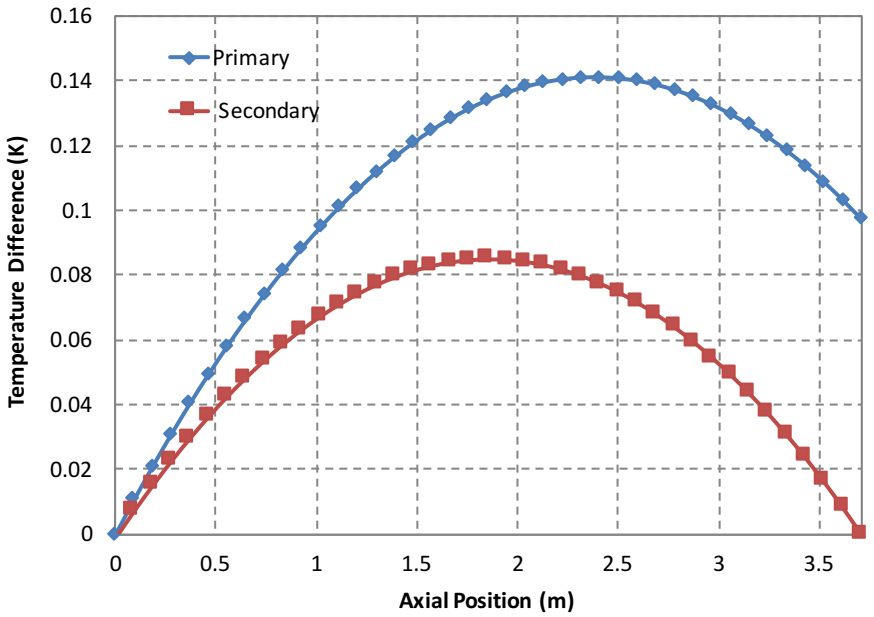

Figure 6-3. Temperature difference between simulations of a cylindrical and a plate tube wall

For completeness, another case (Case 4.2.2) is developed to model a heat exchanger with concurrent flow direction for the two sides. All the other conditions of this heat exchanger are assumed the same as those in Case 4.2.1. The resulting fluid temperature distributions are shown in Figure 6-4. The expected differences between Concurrent and Countercurrent heat exchangers are observed, such as better heat removal in the Countercurrent design and possible maximum cold fluid temperature the Concurrent design.

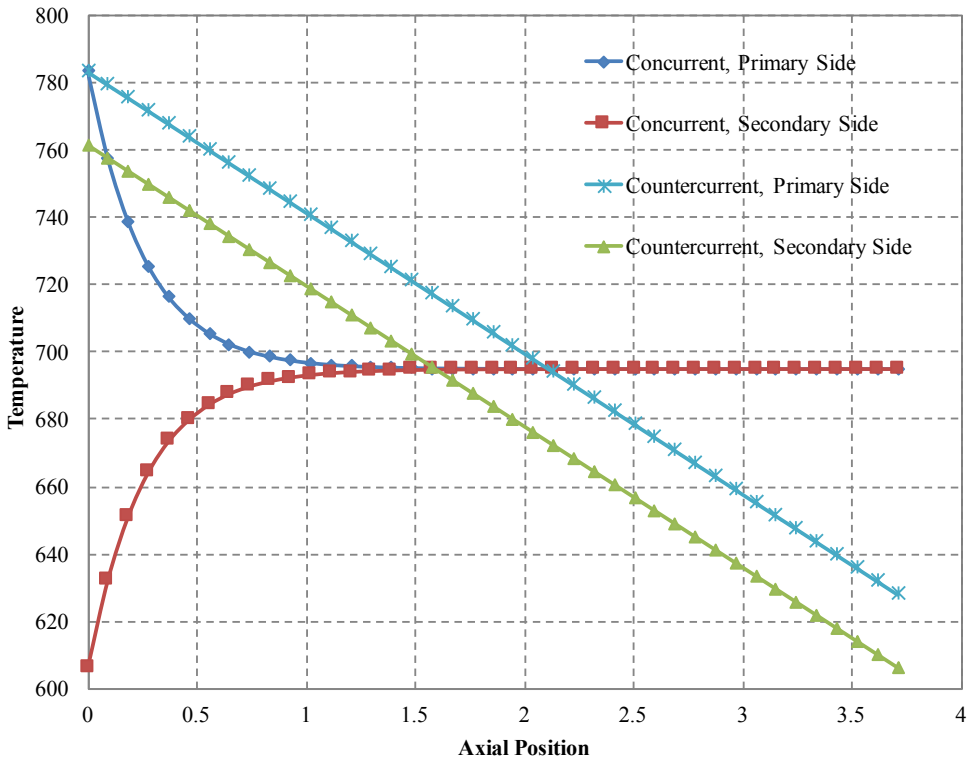

Figure 6-4. Temperature distributions of a Concurrent and a Countercurrent heat exchangers

6.4 Assessment Results Summary

The heat exchanger Component, which simulates the fluid flow in the primary and secondary sides of a heat exchanger, convective heat transfer, and heat conduction in the tube wall, was tested with various configuration, including countercurrent and concurrent heat exchanger with plate or cylindrical tube walls. SAM simulation results were in excellent agreement with the analytical solutions for the Steady test problems, further demonstrating that the basic fluid flow, solid conduction, and convective heat transfer modeling in SAM is accurate.

7 Oscillating U-Tube Manometer

7.1 Introduction

The capability of SAM to predict motion of the interface between liquid and gas in a liquid tank is assessed by the oscillating U-Tube case. Of particular interest is the ability to track the liquid level. An analytical solution for liquid motion in a frictionless U-tube manometer can be obtained from the governing equation of motion for the liquid interface motion derived by Moody [4]. SAM predictions are compared to the analytical solution of the governing equation. The U-tube manometer case is included in the TRACE fundamental validation cases [5].

7.2 Analytical Solution Description

The oscillating manometer is shown schematically in Figure 7-1. It consists of a U-tube shaped frictionless pipe of constant cross-sectional area containing a liquid column of length *L*. The liquid column is set in motion by applying an initial displacement or an initial velocity to the fluid. An exact analytical solution is obtained by Moody for the resulting oscillatory motion, shown in the schematic as *X(t)*. The fluid is assumed to be incompressible so the velocity of the fluid in the entire tube is equal to the time derivative of *X(t)*.

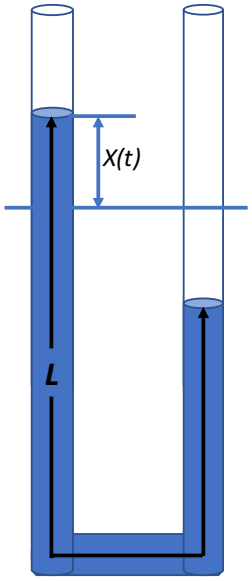

Figure 7-5. Schematic of the Oscillating Manometer

From Moody [4], the displacement *X(t)* satisfies the following equation.

$$\frac{d^2X(t)}{dt^2} + \frac{2g}{L}X(t) = 0 \qquad (7\text{-}1)$$

where *g* is the acceleration of gravity.

With initial conditions of initial displacement of X_0 and initial flow velocity of V_0, the solution of Equation 7-1 is:

$$X(t) = \frac{V_0}{\sqrt{\frac{2g}{L}}} sin\left(\sqrt{\frac{2g}{L}} \cdot t\right) + X_0 cos\left(\sqrt{\frac{2g}{L}} \cdot t\right) \quad (7\text{-}2)$$

The U-tube models both have a constant flow area over their entire length. Hence the liquid velocity is equal to the derivative of the level. That is,

$$V(t) = \dot{X}(t) = V_0 \, cos\left(\sqrt{\frac{2g}{L}} \cdot t\right) - X_0 \sqrt{\frac{2g}{L}} sin\left(\sqrt{\frac{2g}{L}} \cdot t\right) \quad (7\text{-}3)$$

7.3 SAM Model Description

The SAM liquid volume component (*PBLiquidVolume*) is used to model the liquid level moving during the transients. The test problem is modeled by two liquid volumes and three pipes, as shown in Figure 7-6. In the assessment case, the total length of the liquid column is taken as 10 meters, with one meter in the horizontal section of the U-tube. At equilibrium conditions, there will then be 4.5 meters of liquid in each leg, so the equilibrium level is 4.5 meters. The flow area of the tube is taken as 0.0314 m^2. No form or friction losses are included. Two cases were evaluated with different initial conditions:

- Case 5.1: An initial level of 5 m at one leg and 4 m at the other leg, and an initial velocity of $10^{-5}\ m/s$.
- Case 5.2: An initial level of 5 m at one leg and 4 m at the other leg, and an initial velocity of $1\ m/s$ (downward for the leg with high liquid level).

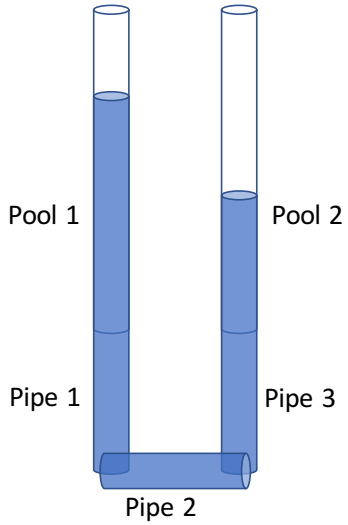

Figure 7-6. SAM model of the oscillating manometer problem

7.4 SAM Simulation Results

The two cases with the initial conditions described above were run for 20 seconds, approximately 4-5 cycles of the oscillation. The analytical solutions were calculated using Microsoft Excel spreadsheet and compared to the SAM solutions. Figure 7-7 shows the Pool 1 liquid level response for Test Case 5.1 with only initial liquid level displacement. The SAM results are indistinguishable from the analytical solution. Figure 7-8 shows the SAM calculated fluid velocity response compared to the analytical solution. The fluid velocities from SAM simulation results agree very well with the analytical solutions. Figure 7-9 and Figure 7-10 show the same comparison for Test Case 5.2 with both an initial liquid level displacement and an initial moving speed of the liquid. Again, the difference between the SAM simulation results and analytical solutions cannot be distinguished on the plots.

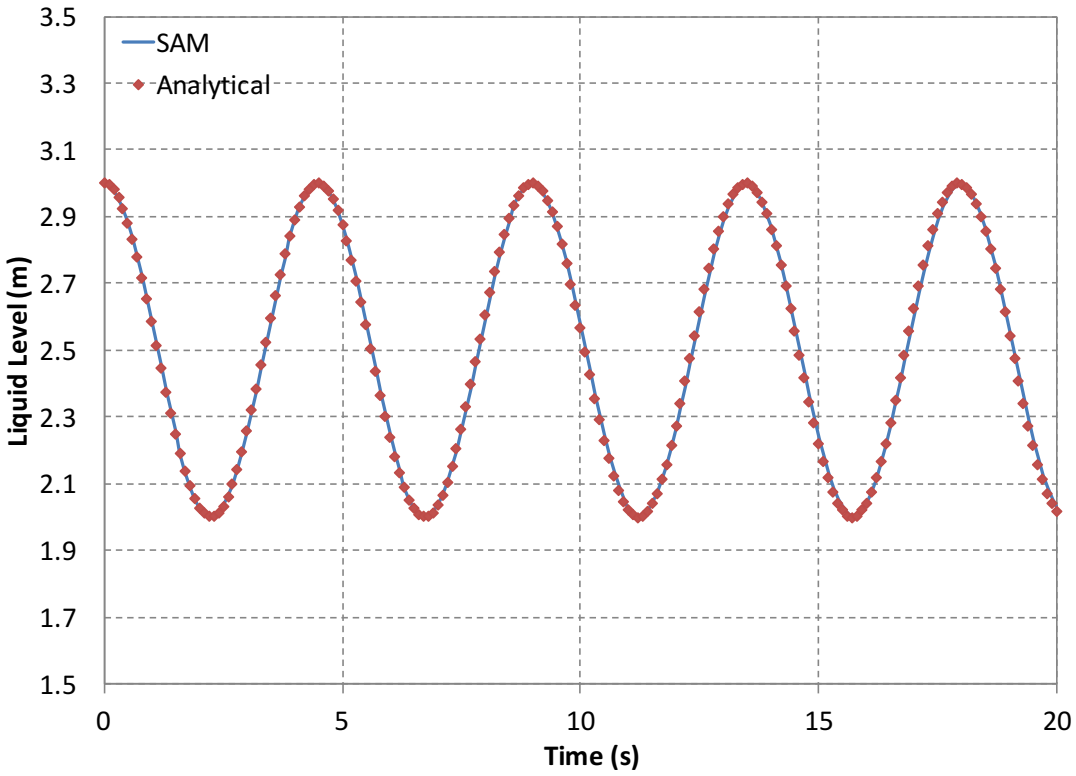

Figure 7-7. Liquid Level vs. Time, Case 5.1

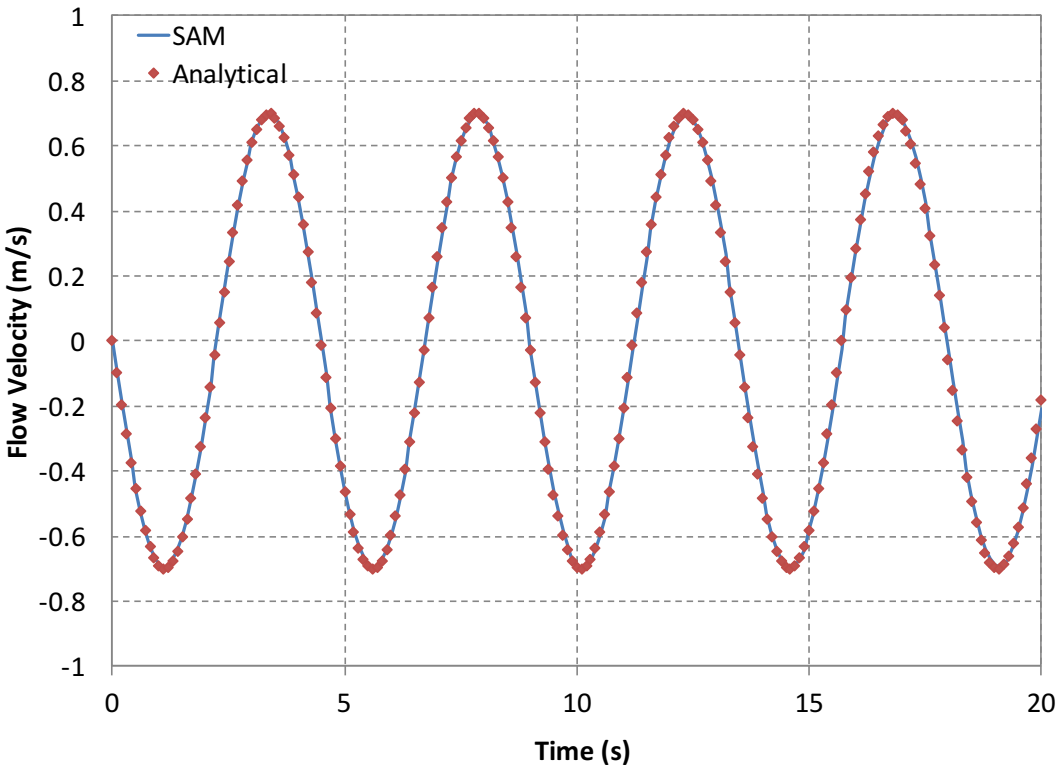

Figure 7-8. Flow Velocity vs. Time, Case 5.1

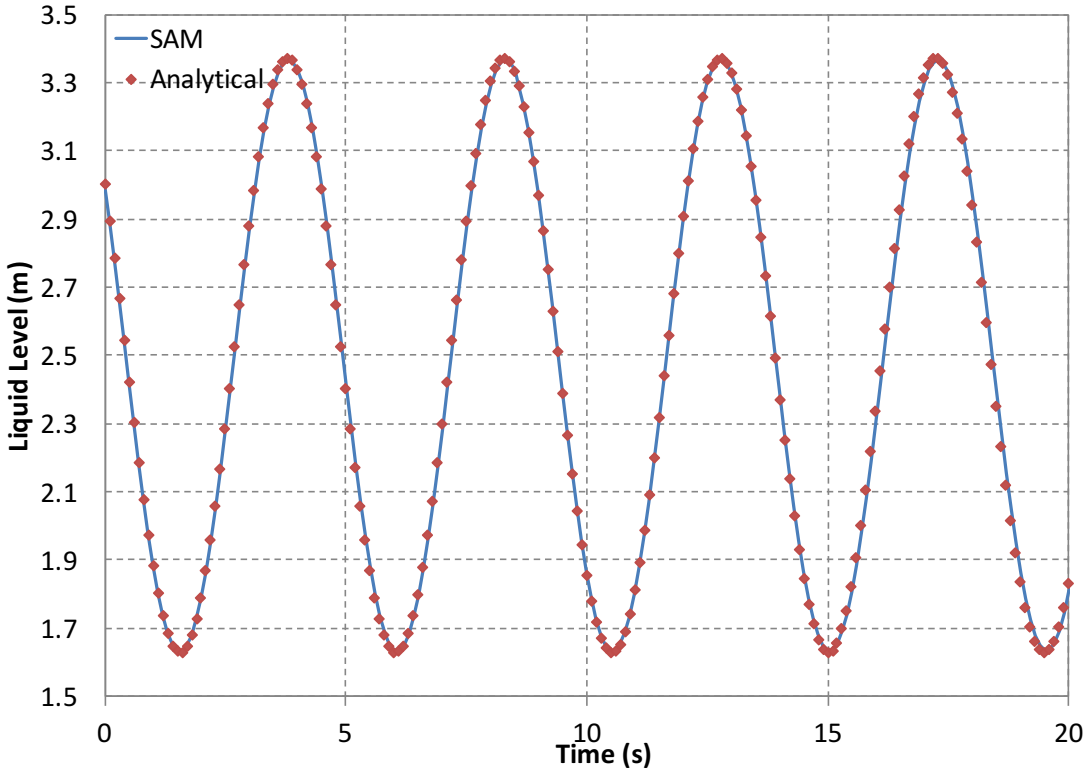

Figure 7-9. Liquid Level vs. Time, Case 5.2

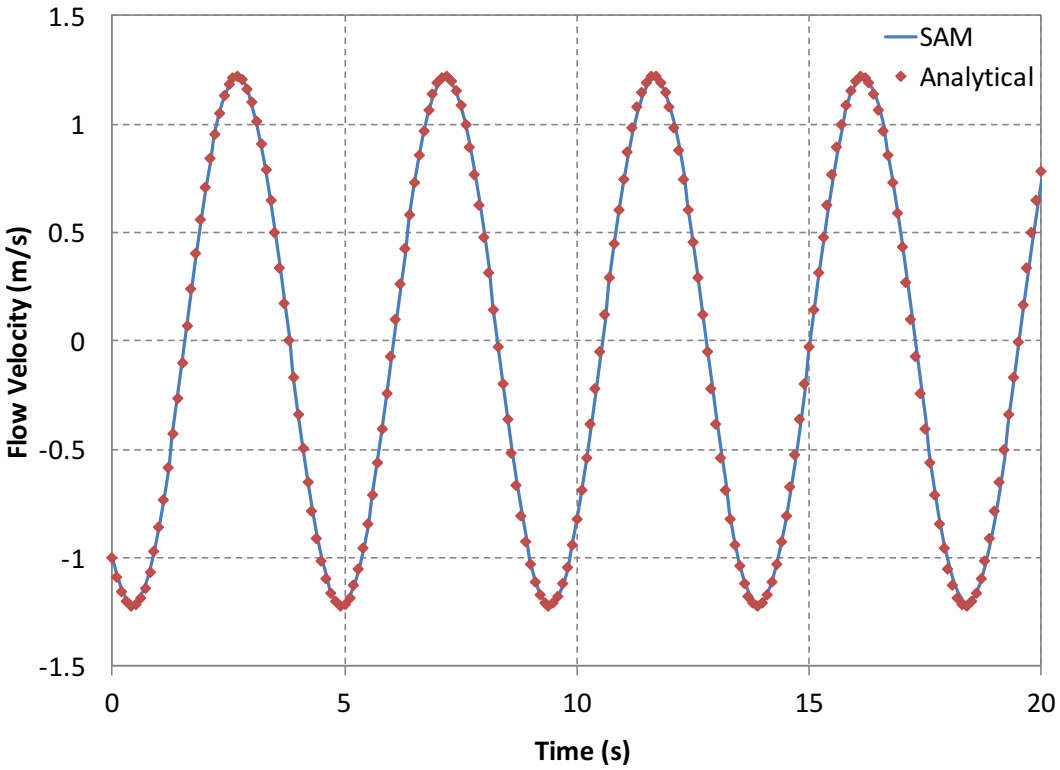

Figure 7-10. Flow Velocity vs. Time, Case 5.2

7.5 Assessment Results Summary

SAM calculations of liquid levels and fluid velocities were compared to the analytical solutions for oscillations in a U-tube manometer. The transient responses calculated by SAM for both test cases with different initial conditions are equivalent to the analytical solutions. Comparing the differences between the code calculations and the analytical results, the Root Mean Square Errors (RMSE) are listed in Table 7-1. It is apparent that the differences between the SAM results and the analytical solutions are insignificant. It should also be noted that a relative coarse mesh ($dx = 0.05\ m$) and large time step size ($dt = 0.05\ s$) were used in SAM simulations. The errors will be reduced if a finer mesh or smaller time step size model are used.

Table 7-1. The Root Mean Square Errors of Simulation Results

Parameters	**Case 5.1**	**Case 5.2**
Level (m)	0.0095	0.016
Velocity (m/s)	0.013	0.023

8 Natural Circulation in a Simple Loop

8.1 Introduction

The purpose of this assessment is to examine SAM capabilities to model a flow loop, as shown in Figure 8-1, with transitions from forced circulation to natural circulation. SAM simulation results will be compared with analytical solutions for initial steady-state and the final equilibrium flow rates under natural circulation cooling.

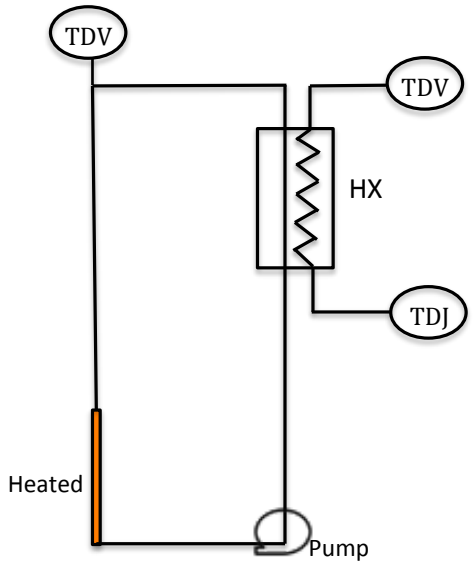

Figure 8-1. Schematics of the loop test problem

8.2 Model Description and Analytical Solution

The simple loop test problem consists of five 1-D pipes (*PBOneDFluidComponent*) and a heat exchanger (*PBHeatExchanger*). One pipe is internally heated, as shown in Figure 8-1. The primary loop (including the heat exchanger) is connected by a set of *PBSingleJunctions* and *PBBranchs*, and a *Pump*. The secondary side of the heat exchanger has fixed inlet velocity and temperature and fixed outlet pressure boundary conditions. The geometric data and operating conditions of the test problem are listed in Table 8-1 and Table 8-2. Note that constant friction coefficients are assumed for all fluid components to obtain an analytical solution of this problem.

Table 8-1. Geometric data of 1-D components

Component	Inlet Elevation (m)	Flow Area (m^2)	Hydraulic Diameter (m)	Length (m)	Friction Coefficient
Pipe 1	0	0.50265	0.8	1	0
Heated Channel	0	0.50265	0.02	1	0.02
Pipe 2	1	0.50265	0.8	2	0
Pipe 3	3	0.50265	0.8	1	0
Pipe 4	2	0.50265	0.8	23	0
HX Primary Side	3	0.50265	0.02	1	0.02
HX Secondary Side	2	0.50265	0.02	1	-

Table 8-2. Additional geometric and operating conditions

Parameters	Values
Heating Power (MW)	322.3
Pump Head (kPa)	10
Heat exchanger heat transfer area (m^2)	502.65
Heat exchanger Tube wall thickness (mm)	1
Heat exchanger secondary flow (kg/s)	3435.6
Heat exchanger secondary inlet temperature (K)	837

Constant fluid properties are assumed for this test problem, except the fluid density which is assumed to be a linear function of fluid temperature. The buoyancy head for this loop can be calculated as:

$$\Delta P_{buoyancy} = \rho \beta g \Delta T (\bar{L}_C - \bar{L}_H) \quad (8\text{-}1)$$

In which $\bar{L}_H$ and $\bar{L}_C$ are the thermal center of the heated section and cooled section in the loop. The friction pressure loss of the loop can be calculated as:

$$\Delta P_{friction} = \sum f \frac{L}{D} \frac{\rho v^2}{2} \quad (8\text{-}2)$$

From energy conservation, the temperature rise in the heated section can be calculated as:

$$\Delta T = \frac{\dot{Q}}{\dot{m} c_p} = \frac{\dot{Q}}{c_p \rho v A} \quad (8\text{-}3)$$

At steady-state, the driving pressure head includes both the pump head and the buoyancy head, and is balanced by the friction pressure loss. The velocity can be calculated by:

$$\beta g \frac{\dot{Q}}{c_p v A}(\bar{L}_C - \bar{L}_H) + P_{pump} = \sum f \frac{L}{D}\frac{\rho v^2}{2} \quad (8\text{-}4)$$

The transient sequence analyzed here is the loss of normal power to the pump. The result is a loss of forced flow in the test loop. In addition, it is assumed that heat removal is available, thus the inlet temperature of the secondary side of the heat exchanger (HX) is assumed constant throughout the transient. The heating power mimics the reactor power during protected loss of flow transient, and decreases to a low power very quickly. The heating power and primary pump head histories, shown in Figure 8-2 and Figure 8-3, were used in this test problem. The flow rates at the secondary side of HX are provided as boundary conditions during the transient, and the normalized flow rates are provided in Figure 8-4.

If the pump is tripped, the velocity under long term natural circulation conditions can be calculated by:

$$v = \left(\frac{2\beta g}{\sum f \frac{L}{D}} \frac{\dot{Q}}{c_p \rho A}(\bar{L}_C - \bar{L}_H) \right)^{1/3} \quad (8\text{-}5)$$

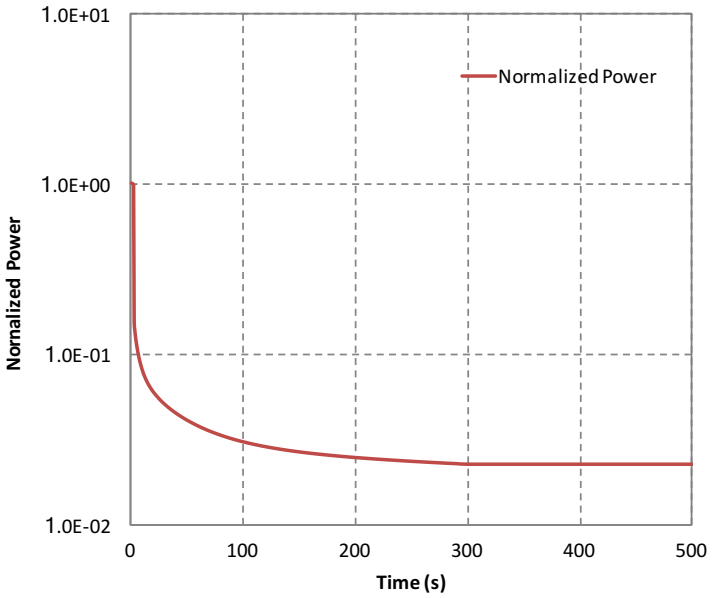

Figure 8-2: Normalized power history during the transient

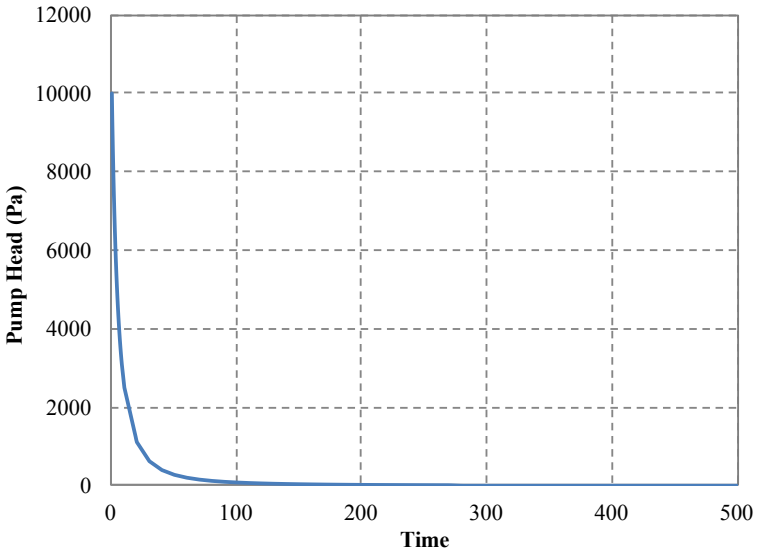

Figure 8-3: Normalized pump head history during the transient

8.3 SAM Simulation Results

A null transient simulation was performed first in SAM to obtain the initial Steady conditions before the pump trip. The restart capability of the SAM code was used to run the transient simulation. The simulation results of the postulated loss-of-protected-flow transient were shown in Figure 8-4 and Figure 8-5.

The pump has sufficient rotating inertia to maintain rotation until about 100 seconds after the start of the transient. This is followed by a transition to natural circulation. Figure 8-4 shows that the transition to natural circulation flow is relatively smooth. Immediately after the transient is initiated, the heating power is rapidly reduced and stays at ~2.26% nominal condition after 300 seconds. At the later part (>100 *s*) of the transient, the HX secondary side flow was reduced to 4% or nominal condition. The heat removal rate at the HX eventually matched the heating power, which lead the system approaching to a new equilibrium state. The transient temperature responses of various locations in the loop are shown in Figure 8-5.

The SAM simulation results of the initial and final steady-state flow rates were compared with the analytical solutions from Equations 8-4 and 8-5. The comparison result is shown in Table 8-3. It was found that SAM simulation result agrees very well with the analytical solution at high flow conditions, indicating the accuracy of both the code simulation and the analytical solutions. However, the agreement was not so good for low-power low-flow conditions. After further examination of the transient simulation results, it was found in Figure 8-6 that the temperature distribution in the HX primary side is no longer linear at the final equilibrium state, because of the very different flow rates in the two sides of the HX. Updating the thermal center of the HX primary side to $z = 2.15\ m$, the resulting analytical solution is very close to the SAM code simulation result.

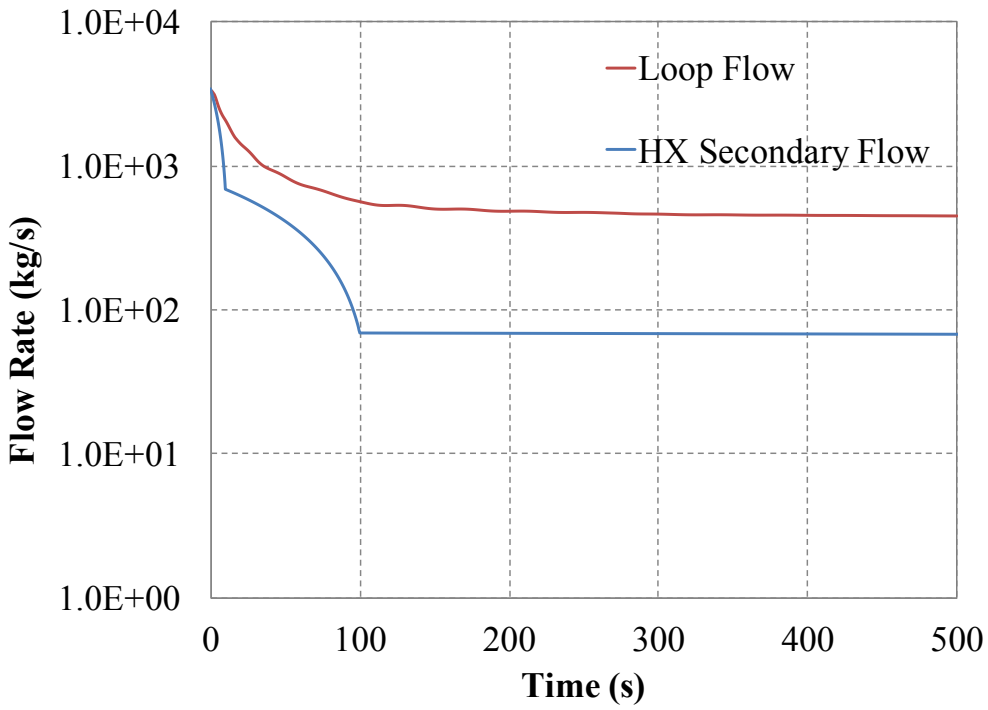

Figure 8-4: Loop and HX secondary side flow rates during the transient

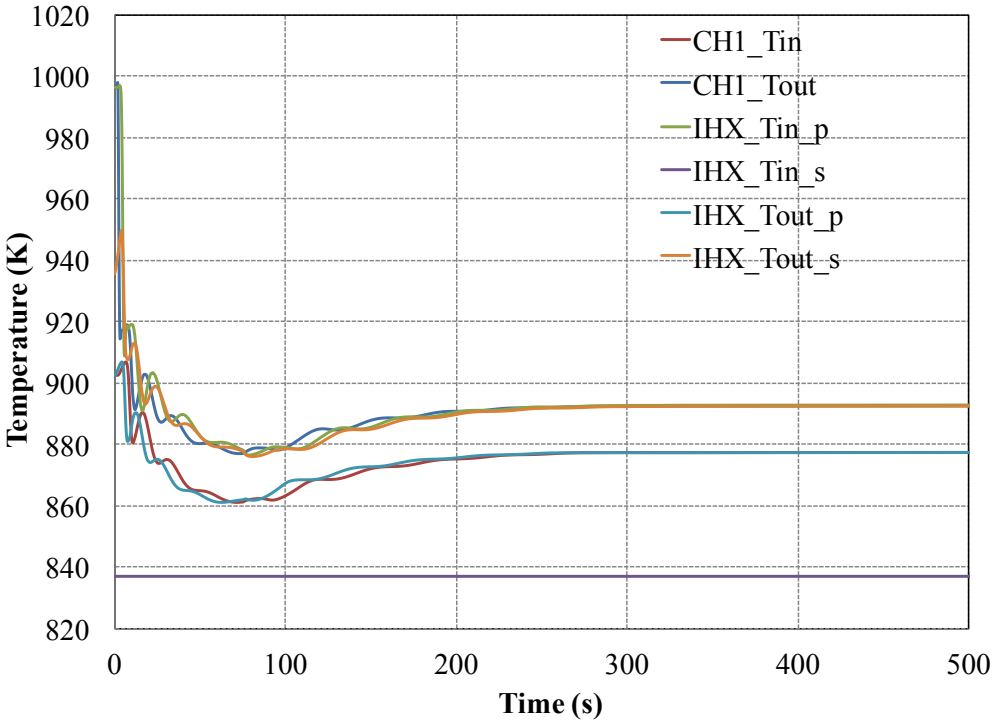

Figure 8-5: Loop temperature responses during the transient

Table 8-3. Comparisons of steady-state flow rates at different conditions

Steady-state flow rate (kg/s)	SAM	Analytical	Difference (%)
With Pump (null transient)	3621	3619	0.04
No Pump (long term natural circulation)	505	536[1]	-6.0
		504[2]	0.2

[1]: thermal center of HX primary side is at the geometric center.
[2]: updated thermal center of HX primary side.

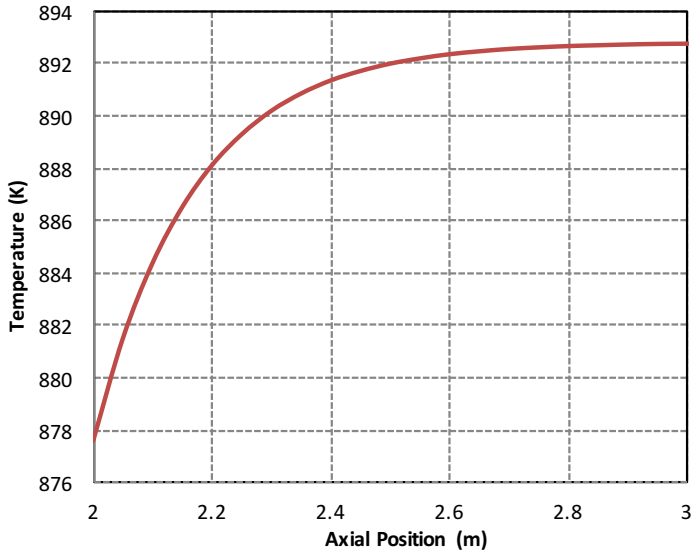

Figure 8-6: Temperature distribution in the HX primary side at the final equilibrium

8.4 Assessment Results Summary

The loop simulation capability in SAM was examined by a simple loop transient problem with transitions from forced circulation to natural circulation. The test mimicked a protected-loss-of-flow transient in a reactor system. SAM simulation results were compared with analytical solutions for initial steady-state and the final equilibrium flow rates under natural circulation cooling. Very good agreements were achieved, demonstrating that the modeling of natural circulation flow in SAM is accurate.

Reference:

1. R. Hu, SAM Theory Manual, Argonne National Laboratory, ANL/NE-17/4, March 2017.
2. B. E. Boyack, M. Straka, and L. W. Ward, TRAC-M VALIDATION TEST MATRIX, Los Alamos National Laboratory, LA-UR-99-6330, May 2001.
3. Y. I. Chang, P. J. Finck, C. Grandy, et al., "Advanced Burner Test Reactor Preconceptual Design Report," ANL-ABR-1 (ANL-AFCI-173), Argonne National Laboratory, September (2006).
4. F. J. Moody, "Introduction to Unsteady Thermofluid Mechanics", John Wiley & Sons, New York, 1990.
5. U. S. Nuclear Regulatory Commission, TRACE 5.0 Assessment Manual - Appendix A: Fundamental Validation Cases, 2008.

Appendix A: Used SAM Components

The physics modeling and mesh generation of individual reactor components are encapsulated as Component classes in SAM for user friendliness. A set of components has been developed for reactor system modeling. The SAM Component used in the six test problems of this assessment are listed and brief described in the table below.

Table A-1. Used SAM Components

Component name	Descriptions	Dimension
PBOneDFluidComponent	Simulates 1-D fluid flow using the primitive variable based fluid model	1-D
PBCoupledHeatStructure	Simulates 1-D or 2-D heat conduction inside solid structures, and connected with liquid components (1-D or 0-D).	1-D or 2-D
PBHeatExchanger	Simulates a heat exchanger, including the fluid flow in the primary and secondary sides, convective heat transfer, and heat conduction in the tube wall.	1-D fluid, 1-D or 2-D structure
PBCoreChannel	Simulates reactor core channels, including 1-D flow channel and the inner heat structures (fuel, gap, and clad) of the fuel rod.	1-D fluid, 1-D or 2-D structure
PBBranch	Models a zero-volume flow joint, where multiple 1-D fluid components are connected.	0-D
PBSingleJunction	Models a zero-volume flow joint, where only two 1-D fluid components are connected.	0-D
PBPump	Simulates a pump component, in which the pump head is dependent on a pre-defined function.	0-D
PBLiquidVolume	A 0-D liquid volume with cover gas (the liquid level is tracked and the volume can change during the transient).	0-D
PBTDJ	An inlet boundary in which the flow velocity and temperature are provided by pre-defined functions.	0-D
PBTDV	A boundary in which pressure and temperature conditions are provided by pre-defined functions.	0-D
ReactorPower	A non-geometric component describing the total reactor power.	ND

Nuclear Engineering Division
Argonne National Laboratory
9700 South Cass Avenue, Bldg. 208
Argonne, IL 60439

www.anl.gov

Argonne National Laboratory is a U.S. Department of Energy laboratory managed by UChicago Argonne, LLC